# Thyroid Hormone Stimulation of Autophagy Is Essential for Mitochondrial Biogenesis and Activity in Skeletal Muscle

Ronny Lesmana, Rohit A. Sinha, Brijesh K. Singh, Jin Zhou, Kenji Ohba, Yajun Wu, Winifred WY. Yau, Boon-Huat Bay, and Paul M. Yen

Laboratory of Hormonal Regulation (R.L., R.A.S., B.K.S., J.Z., K.O., W.WY.Y., P.M.Y.), Program of Cardiovascular and Metabolic Disorders, Duke-National University of Singapore Graduate Medical School, Singapore 169857; Department of Physiology (R.L.), Universitas Padjadjaran, Bandung 45363, Indonesia; Department of Anatomy (Y.W., B.-H.B.), Yong Loo Lin School of Medicine, National University of Singapore, Singapore 117599; and Duke Molecular Physiology Institute and Department of Medicine (P.M.Y.), Duke University Medical Center, Durham, North Carolina 27710, USA

Thyroid hormone (TH) and autophagy share similar functions in regulating skeletal muscle growth, regeneration, and differentiation. Although TH recently has been shown to increase autophagy in liver, the regulation and role of autophagy by this hormone in skeletal muscle is not known. Here, using both in vitro and in vivo models, we demonstrated that TH induces autophagy in a dose- and time-dependent manner in skeletal muscle. TH induction of autophagy involved reactive oxygen species (ROS) stimulation of 5′adenosine monophosphate-activated protein kinase (AMPK)-Mammalian target of rapamycin (mTOR)- Unc-51-like kinase 1 (Ulk1) signaling. TH also increased mRNA and protein expression of key autophagy genes, microtubule-associated protein light chain 3 (LC3), Sequestosome 1 (p62), and Ulk1, as well as genes that modulated autophagy and Forkhead box O (FOXO) 1/3a. TH increased mitochondrial protein synthesis and number as well as basal mitochondrial $O_2$ consumption, ATP turnover, and maximal respiratory capacity. Surprisingly, mitochondrial activity and biogenesis were blunted when autophagy was blocked in muscle cells by Autophagy-related gene (Atg)5 short hairpin RNA (shRNA). Induction of ROS and 5′adenosine monophosphate-activated protein kinase (AMPK) by TH played a significant role in the up-regulation of Peroxisome proliferator-activated receptor gamma coactivator 1-alpha (PPARGC1A), the key regulator of mitochondrial synthesis. In summary, our findings showed that TH-mediated autophagy was essential for stimulation of mitochondrial biogenesis and activity in skeletal muscle. Moreover, autophagy and mitochondrial biogenesis were coupled in skeletal muscle via TH induction of mitochondrial activity and ROS generation. **(*Endocrinology* 157: 23–38, 2016)**

Skeletal muscle is one of the largest tissues in the body. It comprises roughly 40% of whole-body lean mass and needs an efficient method for maintaining its function. Macroautophagy represents the physiological process by which cells sort and specifically directs damaged organelles such as mitochondria to the lysosome for degradation (1). Exercise-induced autophagy has been associated with increased muscle mass, enhanced contractility, and muscle fiber type shifting (2). Therefore, modulating autophagy has been suggested as a key strategy for improving muscle performance as well as treating sarcopenia and several dystrophic muscle diseases (3, 4). On the other hand, autophagic overactivity or overinhibition leads to significant skeletal muscle mass loss, myopathy, muscle injury, and

ISSN Print 0013-7227 ISSN Online 1945-7170
Printed in USA

Received July 21, 2015. Accepted November 2, 2015.
First Published Online November 12, 2015

Abbreviations: PRKAA1/AMPK, 5′Adenosine monophosphate—activated protein kinase; Atg5, autophagy-related gene 5: Baf, bafilomycin $A_1$; BW, body weight; COX, cytochrome oxidase; CQ, chloroquine; EM, electron microscopy; KD, knockdown; 4EBP1, Eukaryotic translation initiation factor 4E-binding protein 1; FOXO, Forkhead box O; GFP, Green flourocense protein; LC3B, microtubule-associated protein light chain 3B; L-NAC, N-acetyl-L-cysteine; mitoTEMPO, 2-(2,2,6,6-tetramethylpiperidin-1-oxyl-4-ylamino)-2-oxoethyl) triphenylphosphonium chloride; OCR, oxygen consumption rate; PPARGC1A, proliferator-activated receptor-γ coactivator 1-α; p70s6 kinase, 70 kDa ribosomal protein S6 kinase 1; QC, quality control; ROS, reactive oxygen species; SERCA2, Sarco/endoplasmic reticulum Ca2+-ATPase, p62, Sequestosome 1; SDHA, Succinate dehydrogenase; PDH, Pyruvate Dehydrogenase; VDAC, Voltage-dependent anion channel; MHC, Myosin Heavy Chain; SRC, spare respiratory capacity; SS, subsarcolemmal; TH, thyroid hormone; shRNA, short hairpin RNA; Ulk1, Unc-51-like kinase 1.

impaired performance (5–9). Therefore, balanced autophagy is critical for maintaining appropriate mitochondrial number and function in skeletal muscle.

Recent studies have highlighted the important role of endocrine regulation of autophagy with examples being testosterone in Sertoli cells, GH in liver, and insulin in skeletal muscle (10–12). Thyroid hormone (TH) also has been shown to induce autophagy to regulate lipid homeostasis (13) and regulate mitochondrial quality control (QC) in liver (14). However, there currently is no information about the role of TH on autophagy in skeletal muscle. TH has been shown previously to regulate the expression of important genes involved in myogenesis, contraction, and regeneration (15–17), as well as mitochondrial activity and biogenesis (18). Additionally, TH has been reported to increase mitochondrial activity by increasing oxygen consumption, substrate oxidation, and the activities of oxidative enzymes (19, 20). Furthermore, TH also is an important regulator of metabolic demand and proper function in skeletal muscle (21). Thus, given the important role of TH in regulating mitochondrial activity in skeletal muscle, we examined TH regulation of autophagy and its potential role(s) in maintaining mitochondrial homeostasis. In the present study, we found that TH stimulates skeletal muscle autophagy both in vitro and in vivo. TH-induced autophagy involved activation of AMPK and ULK1 by mitochondrial reactive oxygen species (ROS) as well as inhibition of mTOR pathway. Moreover, TH-induced autophagy was essential for maintaining mitochondrial activity and biogenesis in skeletal muscle. Our studies have demonstrated a critical feedback system whereby autophagic response to ROS maintains mitochondrial function and number.

## Materials and Methods

### Reagents

$T_3$ (IRMM469–1EA), N-acetyl-L-cysteine (L-NAC) (A7250), bafilomycin $A_1$ (BafA1) (B1793), ((2-(2,2,6,6-Tetramethylpiperidin-1-oxyl-4-ylamino)-2-oxoethyl) triphenylphosphonium chloride, (MitoTEMPO) (CS 1334850-99-5), and chloroquine (CQ) (C6628) were purchased from Sigma-Aldrich. Transfection reagents were procured from Invitrogen. Lentiviral shRNAs Autophagy-related gene (Atg)5 from Dharmacon were used according to manufacture protocols. eGFP/RFP-microtubule-associated protein light chain 3B (LC3B) (Addgene plasmid 21073) plasmids were gifts from Professor T. Yoshimori (Osaka University, Osaka, Japan).

### Animals

Male C57BL/6 mice (2–3 mo old) were purchased and housed in hanging polycarbonate cages under a 12-hour light, 12-hour dark cycle. All mice were maintained according to the Guide for the Care and Use of Laboratory Animals (NIH publication number 1.0.0, revised 2011), and experiments were approved by the Institusional Animal Care and Use Comittees (IACUC)s at Duke-National University of Singapore Graduate Medical School. Hyperthyroidism was induced by injecting $T_3$ at a dose of 20-$\mu$g/100-g body weight (BW) in PBS for 10 consecutive days per ip. Control mice (euthyroid) were injected with PBS alone. CQ was injected at a dose 30-mg/kg BW for 10 days per ip. Animals were killed in $CO_2$ chambers, and blood was drawn by cardiac puncture. Muscle samples were collected according to their muscle type and directly frozen in liquid $N_2$ and stored at −80°C. Samples subsequently were analyzed for protein and RNA expression. Male mice were given fresh drinking water daily containing 1% perchlorate and 0.05% methimazole for 4 weeks to induce hypothyroidism. Fourteen hours before they were killed, all animals were given a sc injection of vehicle (0.9% saline in 100-L volume) for control and hypothyroid group or 40-$\mu$g/100-g $T_4$ with 4-$\mu$g/100-g $T_3$ for hypothyroid + $T_3$/$T_4$ group (22).

### Cell culture

L6 myoblast-derived cell line had been shown as more suitable model for TH study (23). L6 myoblast-derived cells were maintained at 37°C in Dulbecco's Modified Eagle Medium (DMEM) supplemented with 10% fetal bovine serum. After 3 days proliferation with DMEM contained with 10% fetal bovine serum, medium was changed with DMEM contained with 2% Horse Serum (HS) for 5–7 days to induce myotubes formation. For $T_3$ treatment, cells were preconditioned in $T_3$-depleted media (Dowex stripped, 2% horse serum) for 2 days before adding 100nM $T_3$. Control cells were treated with vehicle alone.

### RNA isolation and real-time PCR

Total RNA was isolated and quantitative polymerase chain reaction (qPCR) performed using the QuantiTect SYBR Green PCR kit (204141; QIAGEN) in accordance to the manufacturer's instructions. Actin levels were taken for normalization and fold change was calculated using $2^{-ddCt}$. Primer sequences are provided in Supplementary Table 2.

### Western blotting

Cells or tissue samples were lysed using Radioimmunoprecipitation assay (RIPA) lysis buffer and immunobloting was performed as per the manufacturer's guidelines (Bio-Rad). Densitometry analysis was performed using ImageJ software (National Institutes of Health). Antibodies used for Western blotting are provided in Table 1.

### Gene specific KD using tet-on lentiviral system

For transient transfection L6 myoblast were grown in 6-well plates at a density of $1 \times 10^5$ cells per well. We used special doxycycline-inducible lenti mCMV-turboGFP shRNA Atg5 TCGTTCAGTTATCTCATCC. Cells were transducted with 0.3 Multiplicity of infection (MOI) of $10^{-7}$ lentiviral shRNA (Dharmacon) directed against Atg5 or with a nonsilencing scrambled Enhanced green fluorescent protein (EGFP) negative matched shRNA as control according to the manufacturer's instructions for 48 hours. After puromycin selection for 3 days, we differentiated L6 myoblast become L6 myotubes for 7 days, then L6 cells were incubated with stripped Dowex medium for 48 hours before $T_3$ treatment. Then, L6 cells were incubated with 100nM $T_3$

**Table 1.** Antibodies used for IB and IFA

| Antibody Specificity | Host | Source | Catalog Number | Experiments (Dilution) |
|---|---|---|---|---|
| AMPK$\alpha$1 | Rabbit | Cell Signaling Technology | 2795 | IB (1:1000) |
| Atg5 | Rabbit | Cell Signaling Technology | 2630 | IB (1:1000) |
| Beclin-1 | Rabbit | Cell Signaling Technology | 3738 | IB (1:500) |
| COX IV | Rabbit | Cell Signaling Technology | 4850 | IB (1:1000) |
| GAPDH | Rabbit | Cell Signaling Technology | 2118 | IB (1:3000) |
| LC3B | Rabbit | Cell Signaling Technology | 2775 | IB (1:500) |
| mTOR | Rabbit | Cell Signaling Technology | 2983 | IB (1:1000) |
| p70 S6 kinase | Rabbit | Cell Signaling Technology | 2708 | IB (1:1000) |
| Phospho-4E-BP1 | Rabbit | Cell Signaling Technology | 2855 | IB (1:500) |
| Phospho-AMPK$\alpha$ (Thr172) | Rabbit | Cell Signaling Technology | 4188 | IB (1:1000) |
| Phospho-mTOR | Rabbit | Cell Signaling Technology | 5536 | IB (1:1000) |
| Phospho-p70 S6 kinase | Rabbit | Cell Signaling Technology | 9234 | IB (1:1000) |
| Phospho-ULK1 (Ser555) | Rabbit | Cell Signaling Technology | 5869 | IB (1:1000) |
| Phospho-ULK1 (Ser757) | Rabbit | Cell Signaling Technology | 14202 | IB (1:1000) |
| Pyruvate dehydrogenase | Rabbit | Cell Signaling Technology | 3205 | IB (1:1000) |
| SDHA | Rabbit | Cell Signaling Technology | 11998 | IB (1:1000) |
| SQSTM1/p62 | Rabbit | Cell Signaling Technology | 5114 | IB (1:1000) |
| Tom20 | Rabbit | Cell Signaling Technology | 13929 | IB (1:1000) |
| ULK1 | Rabbit | Cell Signaling Technology | 8054 | IB (1:1000) |
| VDAC | Rabbit | Cell Signaling Technology | 4661 | IB (1:1000) |
| $\beta$-Tubulin | Rabbit | Cell Signaling Technology | 2128 | IB (1:1000) |
| TFEB | Rabbit | Abcam | ab2636 | IB (1:1000) |
| Desmin | Mouse | Thermo Fisher Scientific | MA1-06401 | IB (1:1000) |
| MYOD | Mouse | Thermo Fisher Scientific | MA1-41017 | IB (1:1000) |
| $\beta$-Actin | Mouse | Santa Cruz Biotechnology, Inc | sc-47778 | IB (1:3000) |
| Antigoat IgG-HRP | Donkey | Santa Cruz Biotechnology, Inc | sc-2020 | IB (1:5000–10 000) |
| Antimouse IgG-HRP | Chicken | Santa Cruz Biotechnology, Inc | sc-2954 | IB (1:5000–10 000) |
| Antirabbit IgG-HRP | Chicken | Santa Cruz Biotechnology, Inc | sc-2955 | IB (1:5000–10 000) |

IB, immunoblotting.

for final 24 hours in the present or absent of doxycycline. Puromycin and doxycycline was used according to the manufacture protocols (Dharmacon).

## Mitochondrial oximetry

Oxygen consumption was measured at 37°C using an microplates (type XF24) extracellular analyzer (Seahorse Bioscience). A total of 20 000 of L6 myoblasts cells were seeded at per well in an a XF-24 well culture microplates designed for this instrument, proliferated for 2 days in a 37°C, 10%, $CO_2$ incubator and differentiated become myotubes cells for 7 days before treatment. Optimization of reagents was performed using the Mito stress test kit from Seahorse Bioscience (part number 103015–100) using the protocol and algorithm program in the XF24 analyzer. Basal oxygen consumption rate (OCR) is delta value from OCR with substrates-OCR with rotenone and antimycin A. Adenosine Triphosphate (ATP) turnover corresponds to the OCR used for mitochondrial ATP synthesis and reflects the OCR inhibited by oligomycin. However, ATP could be generated in glycolysis, and oligomycin does not inhibit that. Therefore, here, we use the term "ATP turnover" strictly for ATP generated via oxidative phosphorylation due to the ATP synthase. Maximal OCR or respiratory capacity is [OCR with p-triflouromethoxyphenylhydrazone (FCCP) − OCR with rotenone and antimycin A]. The spare respiratory capacity (SRC) is [OCR with p-triflouromethoxyphenylhydrazone (FCCP) − basal OCR]. After completion of the measurement, assay medium was removed and well contents were lysed in RIPA lysis buffer (Sigma-Aldrich). Protein content in each well was determined by Bio-Rad protein estimation kit.

## Immunofluorescence studies and plasmid transfection

Immunofluorescences experiments were performed as described earlier (14). Cells in all experiment were plated in 96-well plates. For autophagy flux analysis, mRed Flourocense Protein (RPF)-Green Flourocense Protein (GFP)-LC3 plasmid was transfected into L6 cells with Lipofectamine 2000 Transfection Reagent (Invitrogen) at day differentiation 1, and live cell imaging was performed at day differentiation 3 and was performed using an Operetta High Content Imaging System (PerkinElmer) LSM710 Carl Zeiss (Carl Zeiss Microscopy GmbH) confocal microscopy images were obtained from a z confocal plane and quantification was done in single planes.

## Acridine orange staining

Cells were grown on glass coverslips and treated with 100nM $T_3$ for 24 hours. Thereafter, the cells were incubated with 1-$\mu$g/mL Acridine Orange (Sigma-Aldrich) for 15 minutes, fixed for 30 minutes at room temperature at 37°C, and immediately observed under fluorescence microscope and observed using an LSM710 Carl Zeiss confocal microscope.

## Transmission electron microscopy (EM)

Fresh tissue was placed in fixative containing 2% paraformaldehyde and 3% gluteraldehyde in pH 7.4 phosphate buffer

overnight at 4°C. Tissue was washed once in PBS, followed by postfixation with 1% osmium tetroxide. Samples were dehydrated in washes with ascending concentrations of alcohol, followed by embedding in Araldite. Sections were cut and stained with uranyl acetate and lead citrate. Imaging was performed on the Olympus EM208S transmission EM.

### In vivo protein oxidation assay

Protein carbonyl formation as a measure of oxidative stress was measured using an Oxyblot system (S7150; Millipore) according to the manufacturer's instructions.

### Statistics

Individual culture experiments and animal experiments were performed in duplicate or triplicate and repeated 3 times using matched controls, and the data were pooled. Results were expressed as either SD or mean ± SEM. The statistical significance of differences was performed using a 2-tailed Student's *t* test for unpaired observations (comparison of values obtained in 2 groups) or one-way ANOVA followed by a Newman-Keuls multiple comparison test (comparison among 3 or more groups). $P > .05$ considered as not significant.

## Results

### TH induces autophagosome formation, lysosomal activity, and autophagic flux in L6 muscle cells

We used differentiated rat muscle L6 cells (Supplemental Figure 1), to study the effects of TH on autophagosome formation. L6 cells were differentiated into myotubes and then maintained for 3 days in media containing sera stripped of $T_3$ (the active form of TH), and then treated with or without the indicated dose of $T_3$ for 24 hours. Autophagy was monitored using the widely used protein marker, LC3B. When autophagy is increased, LC3B I is lipidated to LC3B II and the amount of LC3B II correlates with the number of mature autophagosomes (24, 25). $T_3$ increased autophagosome amount as evidenced by an increase in LC3B II protein levels in a time- and dose-dependent manner (Figure 1, A–D). $T_3$ increased lysosomal acidification/activity in L6 cells as shown by increased acridin orange staining (Figure 1, E and F). We confirmed these findings in the proliferation phase (L6 myoblast cell) as $T_3$ increased autophagosome formation similar to differentiated L6 cells (Figure 1, G and H). We used L6 cells to study TH regulation of muscle cells because they express high levels of TR. However, in order to confirm that induction of autophagy by $T_3$ was not due to cell line-specific effects, we performed similar experiments in $C_2C_{12}$ myoblasts and primary-cultured mouse myocytes. Induction of autophagy by $T_3$ also was observed in these cells (Supplemental Figure 2).

To analyze $T_3$-induced autophagic flux in L6 cells, we measured another marker, Sequestosome 1 (p62) as well as LC3B II in the absence or presence of lysosomal inhibitors, CQ and Baf. p62 tags ubiquitinated proteins that are targeted to autophagosomes for degradation; thus, a decrease in p62 levels indicates that an increase in autophagic flux occurs due to p62 degradation (Figure 2, A and B). When we used inhibitors of autophagolysosome formation (autophagosome and lysosome fussion), CQ or Baf, we observed an increase in LC3B II levels over baseline control levels. $T_3$ also increased LC3B II levels over baseline control levels; however, more importantly, $T_3$ induced an even greater accumulation of LC3B II in the presence of CQ or Baf, than CQ or Baf alone, suggesting that $T_3$ increased autophagic flux (Figure 2, C–F). We next used tandem fluorescence RFP/GFP-tagged LC3 protein expressed from a chimeric plasmid to examine autophagic flux in our system. In this system, Green Flourocense Protein (GFP) fluorescence is quenched in an acidic environment, and an increase in red fluorescence indicates increased autophagic flux due to autolysosomal formation. We observed increased red fluorescence emission after $T_3$ treatment that was consistent with increased autophagic flux (Supplemental Figure 3).

### TH induces autophagic flux in soleus muscle in vivo

We next examined autophagic flux in vivo in soleus muscle from $T_3$-treated and euthyroid mice (daily ip injections, 20-$\mu$g $T_3$/100-g BW for 10 d). A high dose of $T_3$ was used to induce autophagy in order to maximize changes between the hyperthyroid and euthyroid states. As an index of $T_3$ responsiveness, we analyzed the expression of several known $T_3$ target genes, $Na^+/K^+$-ATPase$\beta$1 and Sarco/endoplasmic reticulum Ca2+-ATPase (SERCA2), and found that their mRNA levels were significantly increased by $T_3$ (Supplemental Figure 4). Similar to our in vitro results, we found that LC3B II protein levels were increased in a time-dependent manner, and p62 protein levels were decreased concomitantly (Figure 3, A–C). Furthermore, we found an increase in autophagosome formation in the subsarcolemmal (SS) area of soleus muscle from $T_3$-treated mice using Electron microscope (EM) (Figure 3, D and E). We also observed that LC3 and p62 mRNA expression were increased in the soleus muscle of mice treated with $T_3$ for 10 days (Figure 3F). In addition, we also observed that $T_3$ increased LC3B II protein levels in other muscles that have mixed fiber type such as vastus lateralis (thigh) and gastrocnemius muscles (Supplemental Figure 5). Finally, in order to rule out the possibility of any thyrotoxic effects on muscle during hyperthyroidism, we examined autophagy in mice treated with methimazole to render them hypothyroid and replaced them with physiological doses of THs (combination 4-$\mu$g/100-g BW of $T_3$ and 40-$\mu$g/100-g BW of $T_4$). We found significant induction of au-

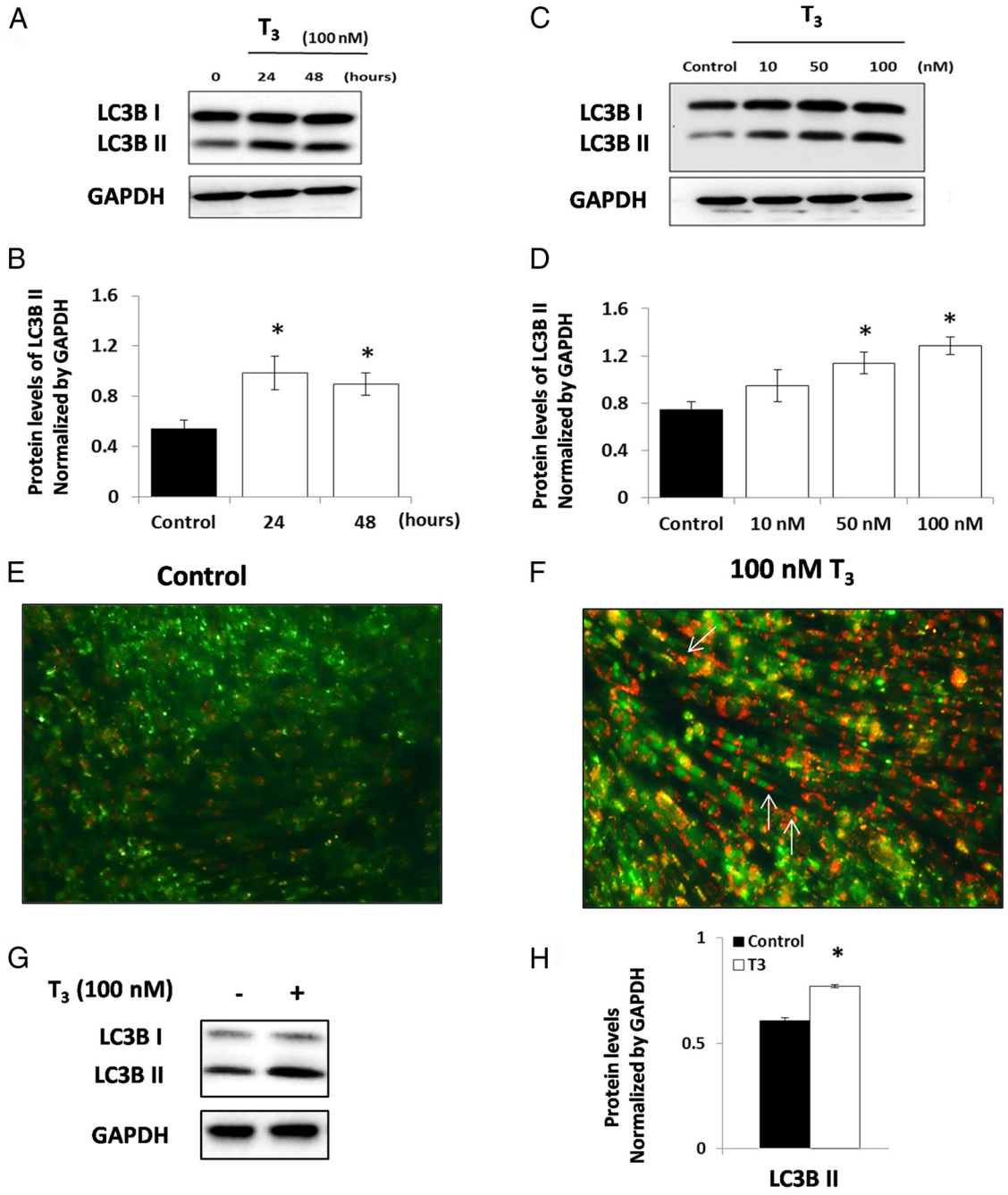


**Figure 1.** $T_3$ increases autophagosome formation in L6 cells. A, Representative immunoblot and quantitation showing treatment of L6 cells with 100nM $T_3$ cells induced autophagosome formation in a time-dependent manner. B, Quantification of densitometry from A. Bars represent the means of the respective individual ratios ± SEM, n = 3; *, $P < .05$. C, Representative immunoblot and quantitation showing L6 myotubes cells treated with different doses of $T_3$ for 24 hours. D, Quantification of densitometry from C (bars represent the mean of the respective individual ratios ± SEM, n = 3; *, $P < .05$) compared with control. E and F, Acridine orange 1-$\mu$g/mL staining of L6 cells in the presence or absence of 100nM $T_3$ for 24 hours showed that $T_3$induced lysosomal acidification. White arrow shows increased lysosome acidification (orange punctuation). G, Representative immunoblot showing treatment of L6 myoblast cells (proliferation phase) with 100nM $T_3$ cells induced autophagosome formation. H, Quantification of densitometry from G. Bars represent the means of the respective individual ratios ± SEM, n = 3; *, $P < .05$.

tophagy when the hypothyroid mice were treated with replacement doses of TH (Supplemental Figure 6).

### TH induces autophagy by activating AMPK and inhibiting mTOR

We then investigated the mechanism underlying $T_3$-induced autophagy in soleus muscle. We observed that $T_3$ activated AMPK by increasing its phosphorylation (Figure 4, A and B). Also, $T_3$ inhibited mTOR signaling as evident by the decreased phosphorylation of mTOR and its downstream targets 70 kDa ribosomal protein S6 kinase 1 (p70s6 kinase), and Eukaryotic translation initiation factor 4E-binding protein 1 (4EBP1) (Figure 4, C–H). Unc-51-like kinase 1 (Ulk1) is the key autophagy initiator that

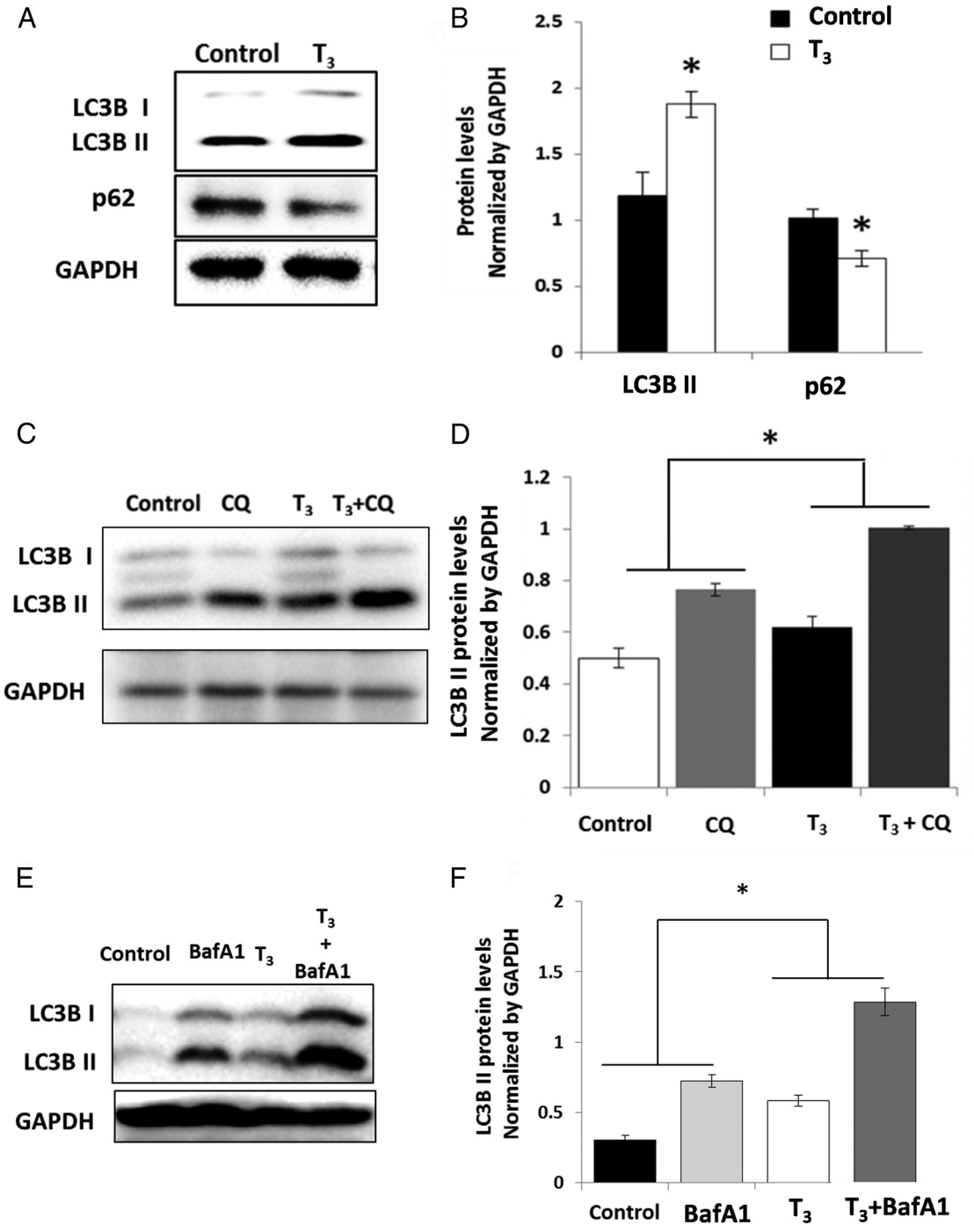


**Figure 2.** $T_3$ increases autophagic flux in L6 cells. A, Representative immunoblot and quantitation showing that treatment of L6 cells with 100nM $T_3$ for 24 hours increased LC3B II protein levels and decreases SQTM1/p62 protein levels, suggesting increased autophagic flux. B, Quantification of LC3B II and p62 densitometries (bars represent the mean of the respective individual ratios ± SEM, n = 3; *, $P < .05$). C, Evaluation of autophagic flux using lysosomal inhibitor, CQ. L6 cells were cotreated with 50$\mu$M CQ for 24 hours in the presence or absence of 100nM $T_3$ for 24 hours. Increase in LC3B II levels of $T_3$-treated cells after CQ cotreatment vs cells treated with either $T_3$ or CQ alone confirmed an increase in autophagic flux. Bars represent the mean of the respective individual ratios ± SEM. D, Quantification of ratio showing net increase in LC3B II. Bars represent the means of the respective individual densitometry of ratios ± SEM, n = 3; *, $P < .05$. E, Evaluation of autophagic flux using lysosomal inhibitor, Baf. L6 cells were cotreated with 30nM Baf for 24 hours in the presence or absence of 100nM $T_3$. Increase in LC3B II levels of $T_3$-treated cells after Baf cotreatment vs cells treated with either $T_3$ or Baf alone confirmed an increase in autophagic flux. F, Quantification of ratio showing net increase of LC3B II. Bars represent the means of the respective individual ratios ± SEM, n = 3; *, $P < .05$.

is activated by AMPK-mediated phosphorylation and inhibited by mTOR-mediated phosphorylation. $T_3$ induced phosphorylation of Ulk1 at the AMPK-targeted site, whereas it decreased phosphorylation at the mTOR-targeted site (Figure 4, I–K). Similar findings for AMPK and mTOR signaling also were seen in L6 cells (Supplemental

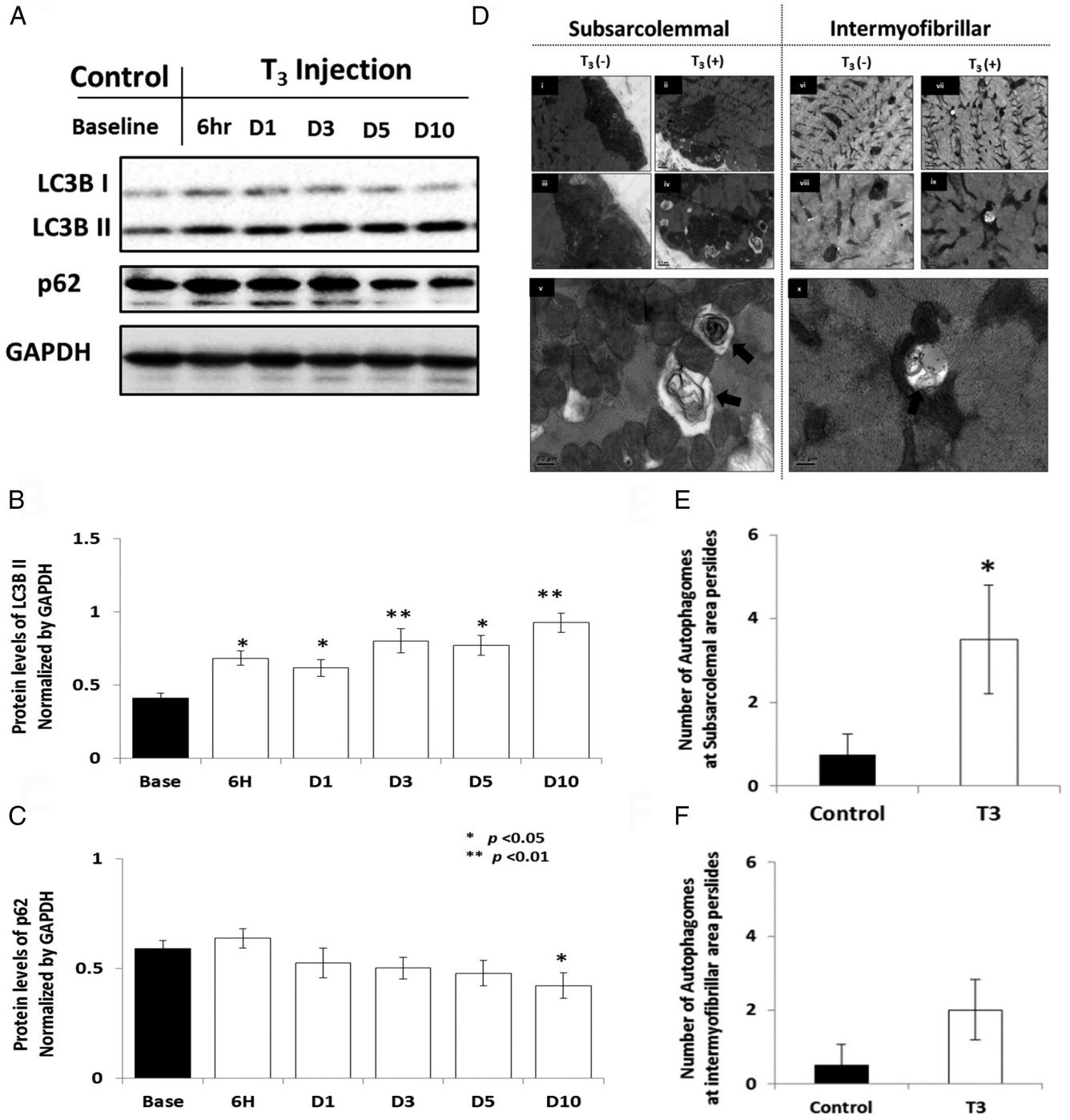


**Figure 3.** $T_3$ increases autophagy flux in soleus muscle. A, Representative immunoblot and quantitation showing time dependency of induction LC3B II and decretion of p62 protein levels in soleus muscle of $T_3$-treated mice (20-$\mu$g $T_3$/100-g BW for 10 d). B and C, Bar graphs show the means of the respective individual ratios ± SEM (n = 5; *, $P < .05$). D, Representative electron micrograph showing $T_3$ induction of autophagosome (AV) formation at SS area of soleus muscle. E, Bar graph showing percentage of AVs in control and $T_3$-treated soleus muscle based on EM micrograph images. Scoring was done by counting 5 random fields per slide condition. Bars represent the means of the respective individual per slide ± SEM (n = 3; *, $P < .05$). F, mRNA expression of LC3B II and p62 genes in soleus muscle of $T_3$-treated mice (20-$\mu$g $T_3$/100-g BW).

Figure 7). In addition, we used the mTOR inhibitor, rapamycin, in combination with $T_3$, and found that it had a synergistic effect with $T_3$ in stimulating autophagy (Supplemental Figure 8).

## TH-induced autophagy is dependent upon ROS

Recent studies have implicated mitochondrial production of ROS as a major regulator of muscle autophagy (26). During oxidative phosphorylation, electron leakage

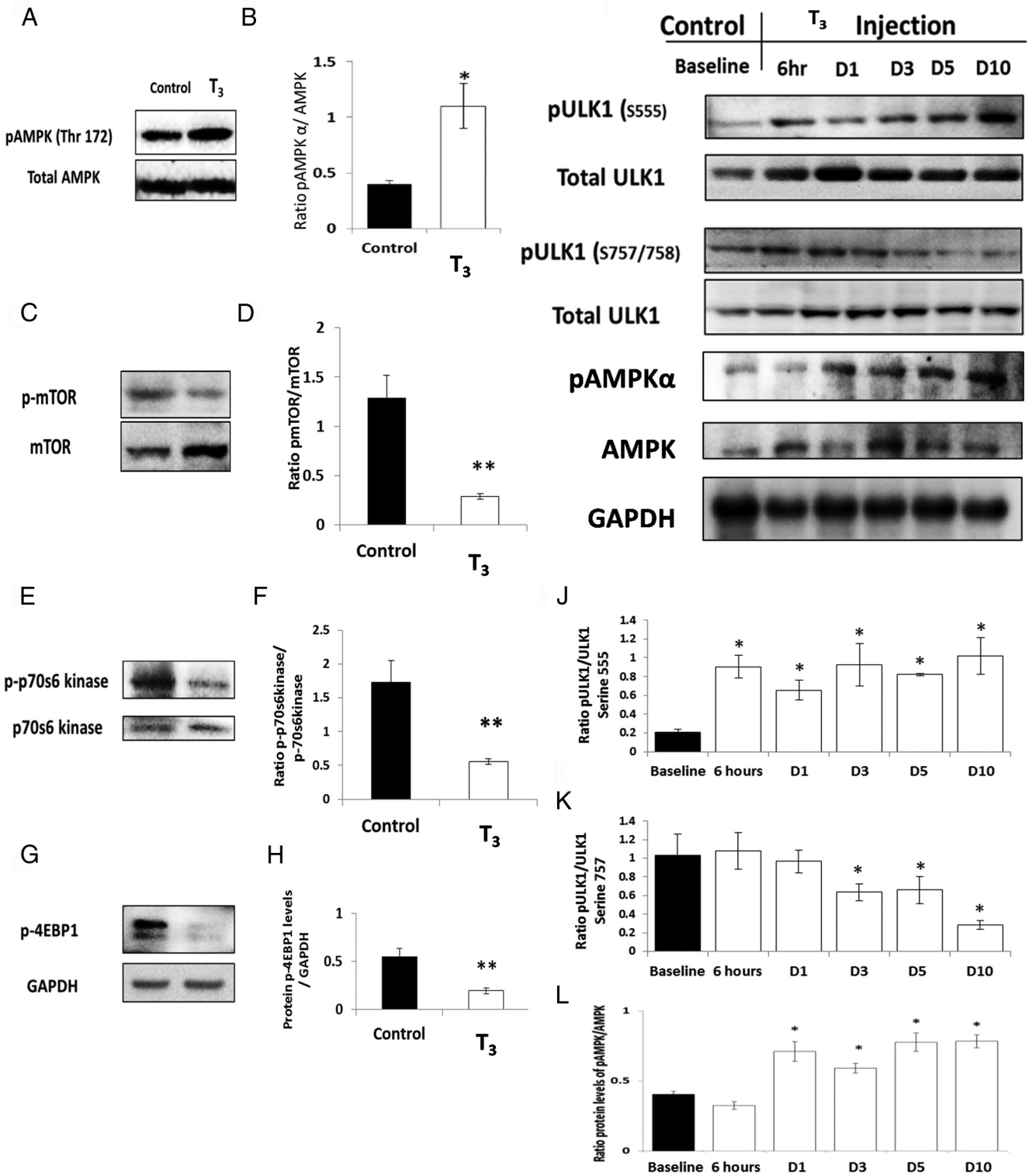


**Figure 4.** $T_3$ regulates autophagy via Ulk1-AMPK-mTOR pathway. A, C, E, and G, Representative immunoblot of AMPK and mTOR phosphorylation, p70s6 kinase, and 4EBP1 from soleus muscle of $T_3$-treated mice (20-$\mu$g $T_3$/100-g BW). B, D, F, and H, Quantification of densitometry ratios for pAMPK/AMPK, mTOR, p70s6 kinase, and 4EBP1. Bars represent the mean of the respective individual ratios ± SEM, n = 5; *, $P < .05$. I, Representative immunoblot of Ulk1 phosphorylation at mTOR and AMPK phosphorylation sites (Ser555 and Ser757/758) from soleus muscle of $T_3$-treated mice (20-$\mu$g $T_3$/100-g BW) that were killed at different time points. J and K, Quantification of densitometry ratio for pUlk1/Ulk1 at Ser555 and Ser757/758. Bars represent the mean of the respective individual ratios ± SEM, n = 5; *, $P < .05$.

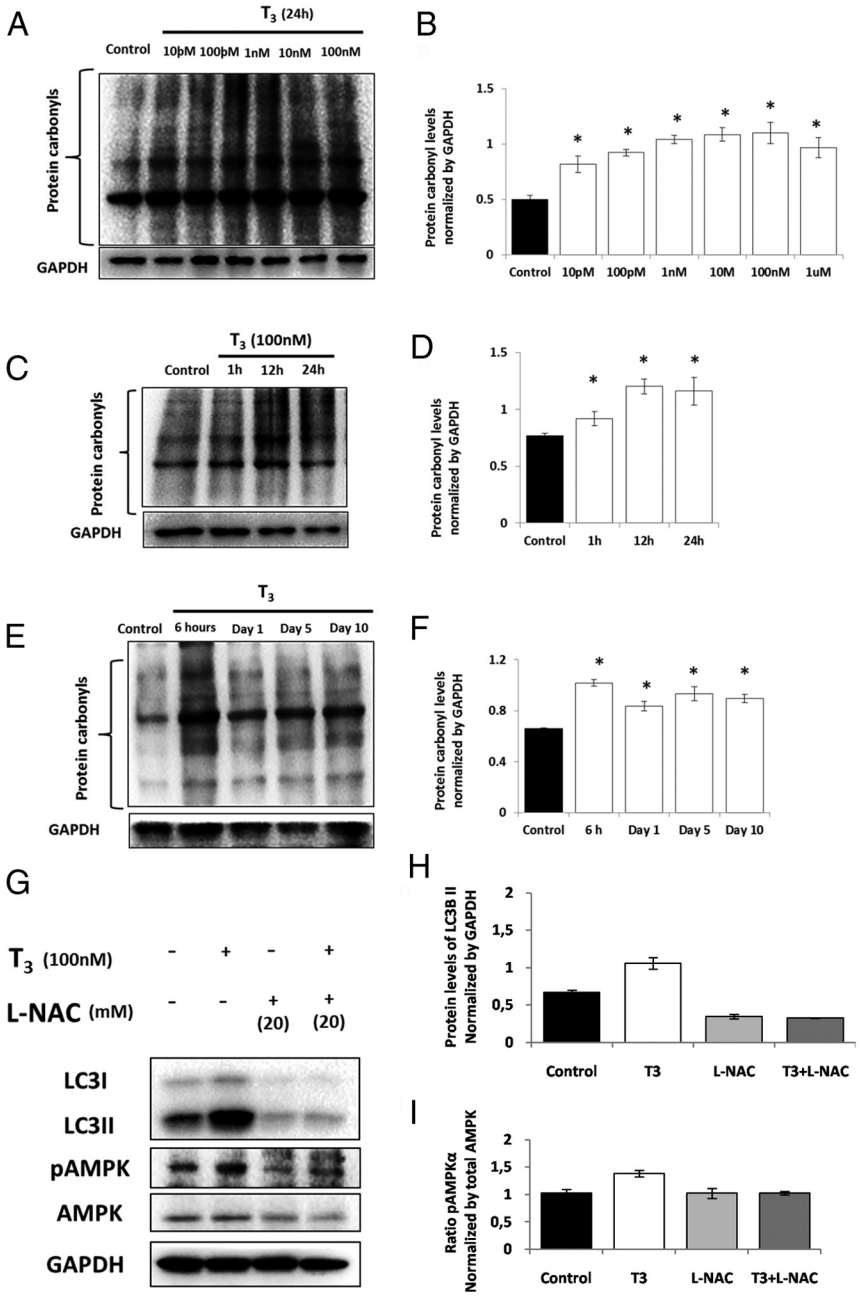


**Figure 5.** Induction of autophagy by $T_3$ is ROS-dependent. A and B, Representative immunoblots showing accumulation of protein carbonyls in time- and dose-dependent manners in L6 cells treated with $T_3$. C, Representative immunoblot showing accumulation of protein carbonyls in time-dependent manner in soleus muscle in mice chronically treated with $T_3$ (20-$\mu$g $T_3$/100-g BW) and killed at different time points. D, Representative immunoblot showing AMPK activation and LC3B II in L6 cells treated with $T_3$ in the absence or presence of the antioxidant, L-NAC. $T_3$ was unable to induce LC3B II formation and AMPK activation in L6 cells treated with L-NAC, suggesting that they are dependent upon ROS formation. E and F, Quantification of LC3B II and AMPK densitometries. Bars represent the means of the respective individual ratios ± SEM, n = 3; *, $P < .05$.

from complex-I and complex-III in electron transport chain produces superoxide anions ($O_2^{\cdot -}$), that generate ROS (27). Because TH previously has been shown to induce mitochondrial activity in skeletal muscle, we examined whether ROS may be coupled with autophagy. Using immunoblot-based detection of carbonyl groups introduced into proteins by oxidative reactions, we assessed the ROS generation in L6 cells treated with $T_3$ and found that ROS production increased in a dose- and time-dependent manner (Figure 5, A and B). In soleus muscle, we also observed that $T_3$ increased protein carbonyl formation due to ROS production (Figure 5C). To demonstrate the essential role of ROS in $T_3$-induced autophagy, we added the antioxidant, L-NAC (pharmaceutical ROS quencher) to $T_3$-treated L6 cells. L-NAC abolished $T_3$-induced AMPK phosphorylation and LC3B II expression, suggesting that ROS had a critical role in mediating $T_3$-induced autophagy (Figure 5, D and E, and Supplemental Figure 9). To determine whether mitochondria were the source for ROS in our system, we used the specific mitochondrial antioxidant (mitoTEMPO) and observed that $T_3$ was unable to induce autophagy in the presence of mitoTEMPO (Supplemental Figure 10).

## $T_3$ regulates the transcription of autophagy genes in skeletal muscle.

Forkhead box O (FOXO) 1 and FOXO3 have been shown to increase transcription of autophagy-related genes and stimulate autophagy (28, 29). We also found that $T_3$ increased *Foxo1* and *Foxo3* mRNA expression in soleus muscle (Figure 6A). Interestingly, $T_3$ increased both mRNA and protein expression of proliferator-activated receptor-$\gamma$ coactivator 1-$\alpha$ (PPARGC1A), a key regulator of autophagy and mitochondrial biogenesis (Figure 6, F and G) (30, 31). Additionally, $T_3$ increased *Ulk1* (Figure 4, I–K), *Atg5*, and *Beclin* mRNA and protein expression levels (Figure 6, C and D). These data suggested that $T_3$ mediated the long-term induction of autophagy and lysosomal genes and their proteins.

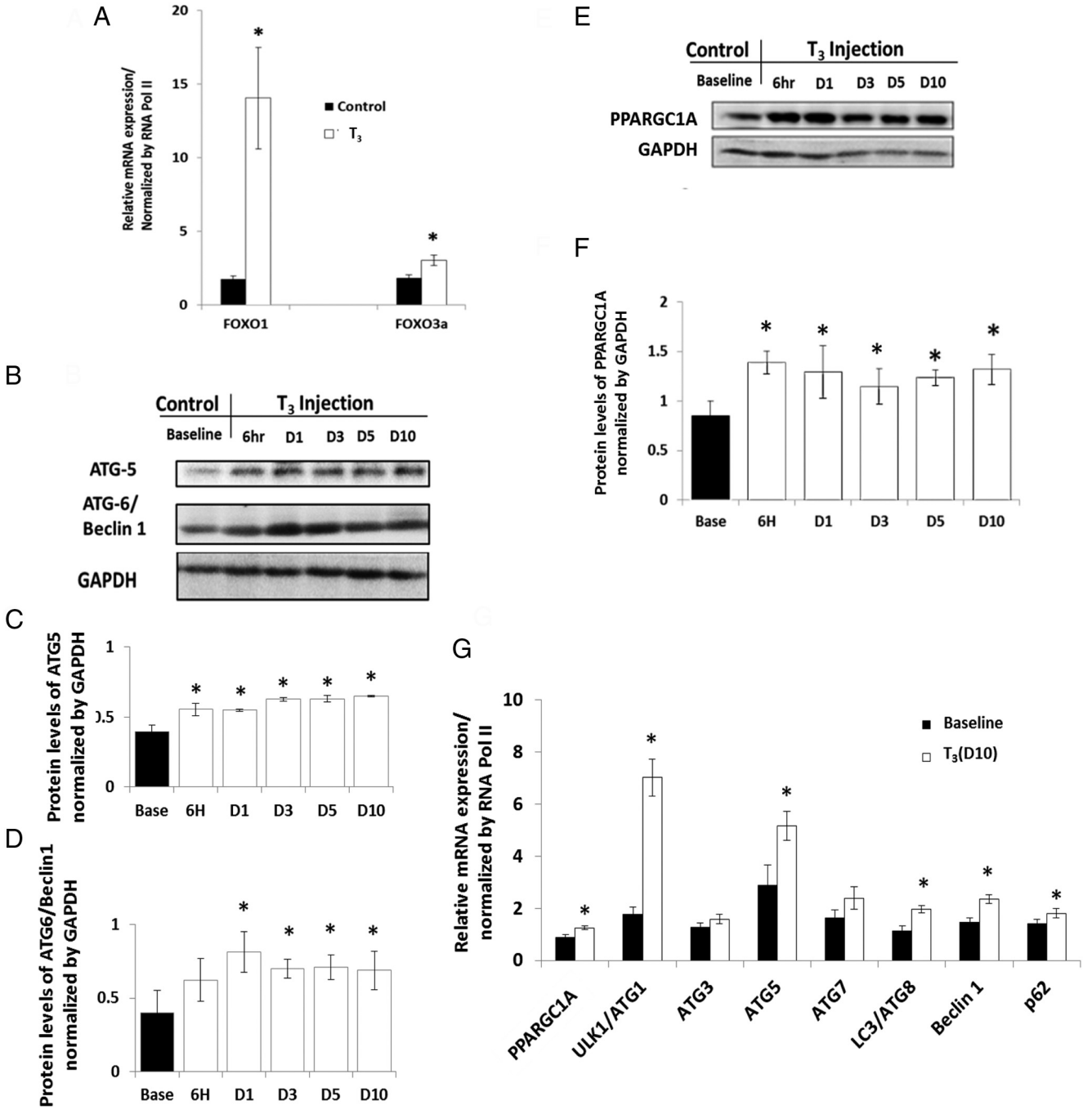


**Figure 6.** $T_3$ increases expression levels of Atg proteins and transcription factors associated with autophagy in soleus muscle. A, Gene expression of FOXO1 and FOXO3 after 10 days of $T_3$ injections. B, Representative immunobots showing the levels of Atg5 and Atg6/Beclin1 in soleus muscle from $T_3$-treated mice that were killed at different time points (20-$\mu$g $T_3$/100-g BW for 10 d). C and D, Bar graphs showing densitometry quantification of data in B. Shown are mean values ± SEM (n = 5). Asterisks (*, $P < .05$) indicate significant differences between $T_3$ treatment alone vs control. E, Representative immunoblot of PPARGC1A proteins from mice treated with 20-$\mu$g $T_3$/100-g BW for 10 days that were killed at different time points. F, Quantification of densitometry ratios. Bars represent the mean values of the respective individual ratios ± SEM, n = 5; *, $P < .05$. H, mRNA expression (ULK1, Atg5, Atg8, and Beclin1), PPARGC1A, and p62 in soleus muscle of mice injected with $T_3$ for 10 days.

## TH induces mitochondrial biogenesis both in vitro and in vivo

We next examined the role of TH on mitochondria biogenesis. Using Cytochrome c oxidase (COX IV) and translocase of outer mitochondrial membranes 20 kDa (TOM20) as markers, we observed that $T_3$ significantly increased these protein levels both in vivo and in vitro (Figure 7, A–C, and Supplemental Figure 11). Electron micrographs of soleus muscle from $T_3$-treated mice also showed increased mitochondrial number both at SS and intermyofibrillar areas of these samples (Figure 7, D–F). Interestingly, we also found increased autophagosome

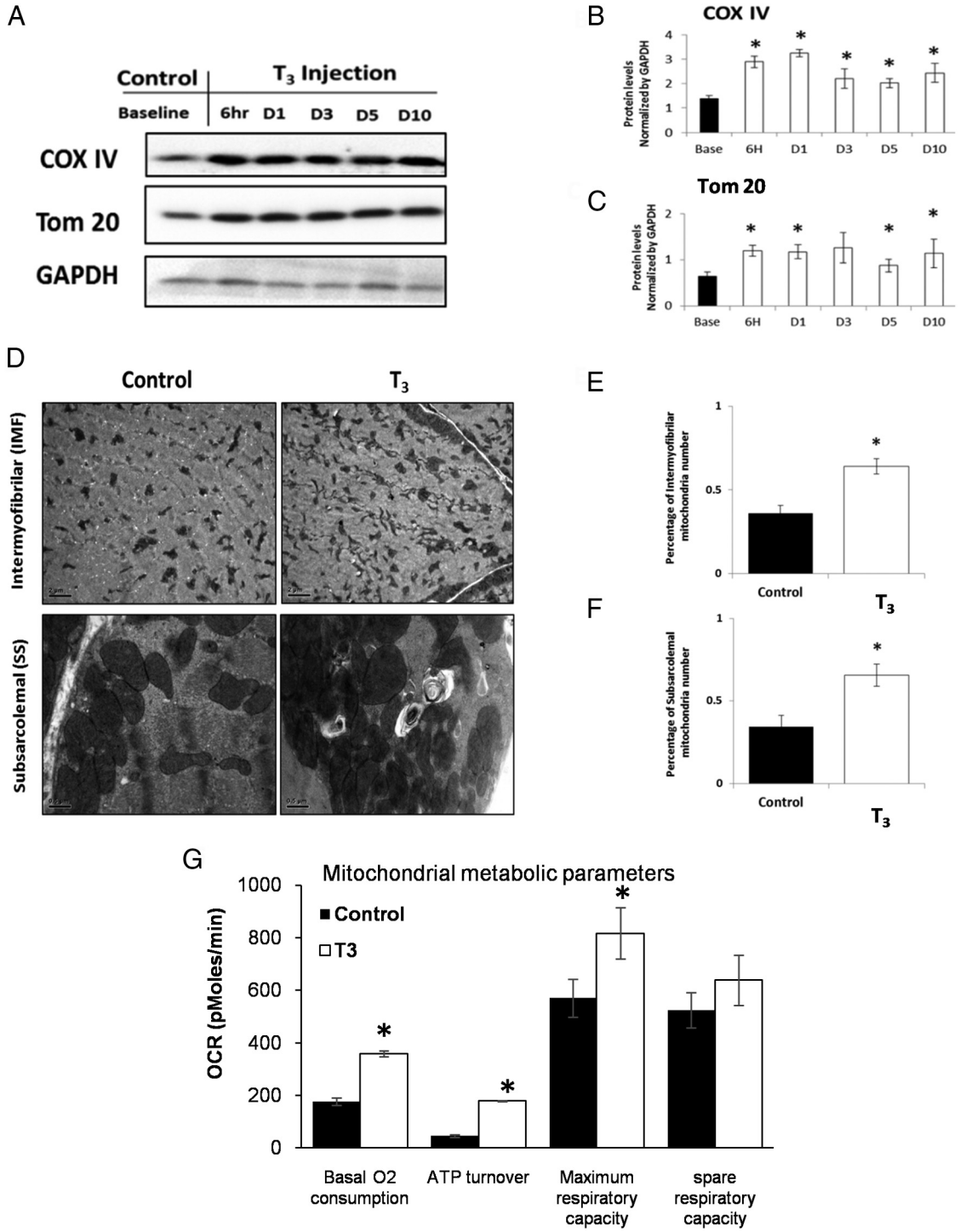


**Figure 7.** Induction of mitochondrial biogenesis and activity by $T_3$. A, Representative immunoblot of TOM20 from soleus muscle of $T_3$-treated mice (20-$\mu$g $T_3$/100-g BW) that were killed at different time points. B and C, Quantification of COX IV and TOM20 densitometries from A. Bars represent the means of the respective individual ratios ± SEM, n = 5; *, $P < .05$. D, Representative electron micrograph of soleus muscle from mice with and without $T_3$ treatment. Arrow shows autophagosome in the area of SS mitochondria. E and F, Quantification of mitochondria number from electron micrographs. Scoring was done by counting 5 random fields per slide condition. Bars represent the means of the group ± SEM, n = 3; *, $P < .05$. G, XF24 Seahorse analyses showing increased basal $O_2$ consumption, ATP turnover, maximum respiratory capacity and Spare capacity in L6 cells treated with 100nM $T_3$.

formation near mitochondria, especially at the SS area in soleus muscle from $T_3$-treated mice (Figure 7D, arrow). Moreover, we analyzed cellular $O_2$ consumption and other parameters of mitochondrial activity in L6 cells during $T_3$ treatment using an extracellular flux analyzer (Seahorse Biosciences). $T_3$ increased basal $O_2$ consumption,

ATP turnover, as well as maximal and SRC in these muscle cells (Figure 7G). These data showed that $T_3$ had general effects on mitochondrial biogenesis and activity of skeletal muscle cells.

### Autophagy regulates $T_3$-induced mitochondrial activity in L6 cells

Recent studies by others and us have shown that autophagy is needed to sustain mitochondrial function during high metabolic demand conditions (14, 31). To determine whether $T_3$-induced autophagy is important for mitochondrial activity, we knocked down Atg5 expression by lentiviral shRNA in L6 cells to block autophagosome formation. As seen previously in Figure 7G, $T_3$ increased basal $O_2$ consumption, ATP turnover, as well as maximal respiratory capacity and SRC consistent with a general increase in overall mitochondrial activity. In contrast, these $T_3$ effects were significantly blunted when Atg5 was knocked down (Figure 8, A–E). These results strongly suggested that $T_3$-induced autophagy was essential for the induction mitochondrial activity by $T_3$. Surprisingly, we found that not only mitochondrial activity but also $T_3$-induced mitochondrial biogenesis was impaired by inhibition of autophagy when Atg5 was knocked down. Immunoblots showed that $T_3$-mediated induction of PPARGC1A and mitochondrial proteins, Succinate dehydrogenase (SDHA), Pyruvate Dehydrogenase (PDH), and Voltage-dependent anion channel (VDAC) protein levels were reduced in L6 cells treated with Atg5 shRNA to block autophagy (Figure 8, F–L). Furthermore, we showed that induction of AMPK phosphorylation by $T_3$ was blunted in L6 cells treated with Atg5 shRNA (Figure 8F), and was associated with loss of PPARGC1A protein induction by $T_3$ (Figure 8, F and N). Additionally, induction of PPARGC1A protein expression depended upon ROS production (Figure 8, M–O). Taken together, these results suggested that both induction of autophagy and mitochondrial biogenesis/activity by $T_3$ are coupled and form a positive feedback loop to increase skeletal muscle mitochondrial function.

## Discussion

Skeletal muscle comprises approximately 40% of body mass in humans and plays a primary role in mediating TH effects on metabolic rate in euthyroidism and dysregulated TH states. TH stimulates ATP consumption by increasing the ATP-generating capacity of skeletal muscle. Although previous studies have described increased mitochondrial biogenesis and energetics by TH in muscle (32), the cell signaling and molecular mechanisms mediating these effects are not well understood. Autophagy was previously regarded as a nonselective cellular degradative process; however, recent studies showed that it also plays a critical role in maintaining mitochondrial health (14). In this connection, skeletal muscle has been shown to rely heavily on autophagy for mitochondrial QC, metabolic plasticity, and energy generation (33–35). In this study, we demonstrated for the first time that $T_3$ stimulates autophagy in skeletal muscle, and surprisingly, $T_3$-mediated mitochondrial activity and biogenesis are coupled with, and dependent upon, autophagy.

We initially showed that $T_3$ increased autophagy in skeletal muscle in both in vitro and in vivo models (Figures 1, A–D, and 3, A–C) similar to its induction of autophagy in liver (13). We then showed that $T_3$ significantly induced autophagic flux in these same models. (Figures 2 and 3, A–C). Next, we showed that $T_3$ up-regulated mRNA and protein expression of several Atg proteins that are important for autophagy such as Atg1/Ulk1, Atg5 and Atg6/Beclin 1 (Figures 3 and 6). Additionally, $T_3$ induced FOXO1 and FOXO3a mRNA expression levels as well as PPARGC1A (Figure 6, A–F). These transcription factors contribute to the autophagic process and lysosome synthesis in skeletal muscle (36, 37).

Our results also showed that induction of autophagy by $T_3$ was tightly linked to its effects on mitochondrial biogenesis and activity. In this regard, our data is in agreement with previous studies showing a similar relationship between autophagic induction and mitochondrial function during exercise (6, 38). We observed that $T_3$ increased mitochondria number both in vitro and in vivo based upon EM imaging and increased expression of mitochondrial proteins in cell extracts. Additionally, PPARGC1A mRNA and protein were induced by $T_3$. This transcriptional factor plays a critical role in mitochondria biogenesis (30, 39). $T_3$ also increased overall mitochondria activity in differentiated L6 myotube cells analyzed by oximetry (Figure 7I).

Our results further suggested that induction of autophagy by $T_3$ depended upon mitochondrial activity. We showed that increased mitochondrial ROS production is a major driver of $T_3$-induced autophagy via activation of the AMPK pathway. In particular, $T_3$ induced ROS generation in a time- and dose-dependent manner, which was accompanied by increased autophagosome formation in $T_3$-stimulated L6 cells. This stimulation of autophagy was abrogated by coadministration of the ROS inhibitors, L-NAC or mitoTEMPO with $T_3$. A similar mechanism has also been proposed for other stress conditions affecting skeletal muscle (40–42) and suggests that mitochondrial ROS is a critical mediator of autophagy in this tissue.

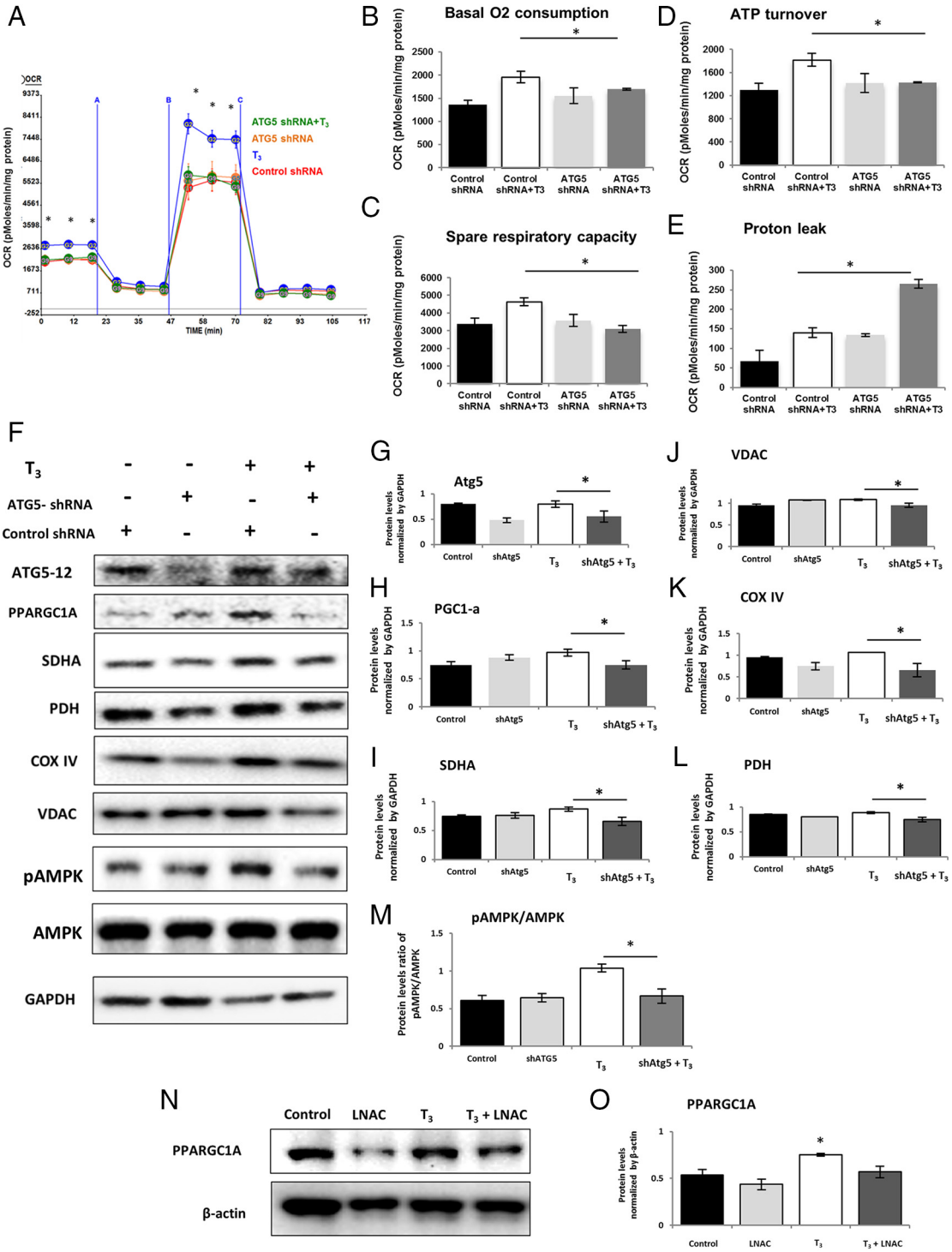


**Figure 8.** Inhibition of $T_3$-induced autophagy impairs mitochondrial biogenesis and activity and is associated with decreased. PPARGC1A expression. A, Seahorse analysis of oxygen consumption in $T_3$ (100nM/24 h)-treated L6 myotube cells transformed with lentiviral *Atg5* shRNA or scrambled control shRNA. OCR was measured as described in Materials and Methods. B–E, Representative plot basal/maximal respiration as well as SRC in $T_3$ (100nM/24 h)-treated L6 myotube cells. Bars represent the mean of the respective individual ratios ±SD (n = 5). The asterisk (*, $P < .05$) indicates difference compared between $T_3$ alone vs control and (#, $P < .05$) indicates difference between cells treated with $T_3$ + Atg5 shRNA vs $T_3$ + scrambled control shRNA. F–M, Representative immunoblot and densitometry quantifications showing effects of KD efficiency of Atg5 in the presence or absence of $T_3$ on Atg5, PPARGC1A, VDAC, COX IV, SDHA, PDH, LC3B II, and AMPK in L6 cells. Quantification of pAMPK/AMPK densitometry ratios are shown (bars represent the mean of the respective individual ratios ± SEM, n = 3; *, $P < .05$). N, Representative immunoblot showing ROS is necessary for induction of PPARGC1A in L6 cells treated with $T_3$ in the absence or presence of L-NAC. O, Quantification of densitometry from PPARGC1A normalized by $\beta$-actin (bars represent the mean of the respective individual ratios ± SEM, n = 3; *, $P < .05$).

AMPK activation has been reported to be associated with stimulation of autophagy in skeletal muscle (43). Similarly, we observed that $T_3$ induced AMPK phosphorylation in soleus muscle and L6 cells (Figure 4). AMPK promotes autophagy by directly activating Ulk1 through phosphorylation of Ser317 and Ser777 (44, 45). This Ulk1 phosphorylation then initiates autophagy. In this connection, we previously reported that $T_3$-induced autophagy required Ulk1 phosphorylation by AMPK in the liver (14). mTOR activation also leads to phosphorylation of Ulk1 at a different site (Ser757); however, this phosphorylation has an opposite effect and inhibits autophagy by disrupting the interaction between Ulk1 and AMPK (44, 45). In our studies, we observed that phosphorylation of Ulk1 was increased at the AMPK site and concomitantly decreased at the mTOR site in soleus muscle from $T_3$-treated mice (Figure 4, I–K). The mTOR pathway previously was shown to have an important role in regulating autophagy in skeletal muscle and controlling muscle mass (7). In this connection, we found that $T_3$ inhibition of mTOR phosphorylation not only decreased the inhibition of Ulk1, but also decreased the phosphorylation of its downstream targets, p70s6 and 4EBP1 (Figure 4, A–H).

Alteration in thyroid status is associated with changes in mitochondrial mass, structure, and contraction capability (46). Moreover, autophagy regulates mitochondrial homeostasis (38). We observed that $T_3$ increased mitochondria number in skeletal muscle by EM (Figure 7, D–H). Interestingly, we also noticed increased autophagosome formation near mitochondria in the SS areas of soleus muscle from $T_3$-treated mice (Figure 7D). In further support of a critical role for $T_3$-mediated autophagy in regulating mitochondrial number and function, we observed that Atg5 knockdown (KD) in L6 cells with shRNA lentivirus led to blunting of $T_3$-stimulated expression of mitochondrial proteins such as cytochrome oxidase (COX) IV, VDAC, SDHA, and PDH (Figure 8, F–L). Moreover, $T_3$-mediated induction of basal metabolic rate, ATP turnover, and maximum respiration rate in mitochondria were abolished by KD of Atg5 expression (Figure 8, A–E). The dependence on autophagy by both $T_3$-induced mitochondrial activity and biogenesis was further demonstrated by our observation of decreased induction of PPARGC1A protein by $T_3$ that was associated with decreased phosphorylation of AMPK after Atg5 KD in muscle cells (Figure 8, F, H, and M). Because AMPK induction was mediated by ROS (Figure 5, D and F), it is noteworthy that inhibition of ROS also led to decreased PPARGC1A protein expression (Figure 8N). Thus, ROS generated from increased oxidative phosphorylation by $T_3$ may control both autophagy and mitochondrial biogenesis through stimulation of AMPK phosphorylation (Supplemental Figure 12). This AMPK activation then leads to phosphorylation of Ulk1 and stimulation of autophagy as well as induction of PPARGC1A and increased mitochondrial synthesis. It is likely that TH-mediated mitophagy also contributes to maintaining mitochondrial QC and function, because inhibition of autophagy by Atg5 shRNA blocks mitochondrial activity induced by $T_3$. In this connection, we recently showed that $T_3$ stimulates mitophagy in the liver (14). Further studies will be needed to clarify the precise mechanism by which autophagy induces mitochondrial biogenesis through PPARGC1A.

TH regulates metabolic demand and drives tissues to use fuel selectively (47). TH also increases maximal oxygen consumption and the activities of citrate synthase and COX consistent with a change in skeletal muscle fiber type in response to its fuel demands (39). Indeed, it previously was shown that $T_3$ can alter cardiac and skeletal muscle fiber ratios by decreasing $\beta$MHC/MHCI and increasing MHCIIa (48). Studies in deiodinase 2 Knock out-mice in which intracellular $T_3$ concentrations in skeletal muscle were decreased due to decreased $T_4$ to $T_3$ conversion further support the role of TH in determining muscle fiber type and activity (49). Thus, it is noteworthy that we also observed a decrease in oxidative MHCI and an increase in glycolytic MHCIIa fibers accompanying the $T_3$-mediated increase in mitochondrial activity and biogenesis observed in both soleus skeletal muscle and differentiated L6 cells, and this process may have a tight association with autophagy, especially for MHCI (Supplemental Figure 13). These findings suggest that changes in mitochondrial activity, muscle fiber type, and fuel use (from oxidation of fatty acid to glycolysis) are associated with the $T_3$-mediated increase in autophagy and mitochondrial biogenesis.

In summary, our data demonstrate that $T_3$ stimulates mitochondria biogenesis and activity via autophagy in skeletal muscle. Homeostasis of mitochondrial function, biogenesis, and turnover are important factors that determine skeletal muscle performance and fiber adaptation, and are regulated by TH via autophagy. Thus, diseases that affect muscle performance such as muscular dystrophies and myopathies (50, 51) as well as degenerative conditions such as sarcopenia in aging may potentially be treated by stimulation of mitochondrial biogenesis and activity by $T_3$ or its analogs, particularly because TH induces transcription of PPARGC1A mRNA as we and others have observed (52, 53). Additionally, reduced autophagy has been linked to decreased mitochondrial biogenesis in these and other degenerative conditions (54–56). Thus, our finding that TH-mediated autophagy also stimulates mitochondrial biogenesis opens the possibility that activation of autophagy itself or in combination with

$T_3$ may be a novel therapeutic strategy for these conditions.

## Acknowledgments

We thank Mr Benjamin L. Farah, Sherwin Xie, Ms Andrea Lim, Mr Joel Lee Yi Ji, and Ms Chong Shu Yun for their helpful technical supports.

Address all correspondence and requests for reprints to: Professor Paul M. Yen, M.D., Laboratory of Hormonal Regulation, Cardiovascular and Metabolic Disorder Program, Duke-National University of Singapore Graduate Medical School, 8 College Road, Singapore, 169857. E-mail: paul.yen@duke-nus.edu.sg.

This work was supported by Duke-National University of Singapore Graduate Medical School Faculty Start-up Funds, sponsored by the Ministry of Health, Ministry of Education, and Ministry of Trade, Singapore; A*StaR and NMRC Grant EDG10nov012; NMRC/Clinician Scientist Award/0054/2013; NMRC/CIRG/1340/2012 (to P.M.Y.) from the Ministry of Health, Singapore; DIKTI-KLN international collaboration grant (R.L.) from Ministry of Education and Research, Indonesia; the and NMRC Grant NMRC/BNIG/2025/2014 (to R.A.S.).

Disclosure Summary: The authors have nothing to disclose.

## References

1. **Mizushima N, Komatsu M.** Autophagy: renovation of cells and tissues. *Cell*. 2011;147:728–741.
2. **Tam BT, Pei XM, Yu AP, et al.** Autophagic adaptation is associated with exercise-induced fibre-type shifting in skeletal muscle. *Acta physiol (Oxf)*. 2015;214:221–236.
3. **Grumati P, Coletto L, Sabatelli P, et al.** Autophagy is defective in collagen VI muscular dystrophies, and its reactivation rescues myofiber degeneration. *Nat Med*. 2010;16:1313–1320.
4. **De Palma C, Morisi F, Cheli S, et al.** Autophagy as a new therapeutic target in Duchenne muscular dystrophy. *Cell Death Dis*. 2012;3:e418.
5. **Thapaliya S, Runkana A, McMullen MR, et al.** Alcohol-induced autophagy contributes to loss in skeletal muscle mass. *Autophagy*. 2014;10:677–690.
6. **Lira VA, Okutsu M, Zhang M, et al.** Autophagy is required for exercise training-induced skeletal muscle adaptation and improvement of physical performance. *FASEB J*. 2013;27:4184–4193.
7. **Castets P, Lin S, Rion N, et al.** Sustained activation of mTORC1 in skeletal muscle inhibits constitutive and starvation-induced autophagy and causes a severe, late-onset myopathy. *Cell Metab*. 2013;17:731–744.
8. **Masiero E, Sandri M.** Autophagy inhibition induces atrophy and myopathy in adult skeletal muscles. *Autophagy*. 2010;6:307–309.
9. **Raben N, Hill V, Shea L, et al.** Suppression of autophagy in skeletal muscle uncovers the accumulation of ubiquitinated proteins and their potential role in muscle damage in Pompe disease. *Hum Mol Genet*. 2008;17:3897–3908.
10. **Ma Y, Yang HZ, Xu LM, Huang YR, Dai HL, Kang XN.** Testosterone regulates the autophagic clearance of androgen binding protein in rat Sertoli cells. *Sci Rep*. 2015;5:8894.
11. **Zhang Y, Fang F, Goldstein JL, Brown MS, Zhao TJ.** Reduced autophagy in livers of fasted, fat-depleted, ghrelin-deficient mice: reversal by growth hormone. *Proc Natl Acad Sci USA*. 2015;112:1226–1231.
12. **Naito T, Kuma A, Mizushima N.** Differential contribution of insulin and amino acids to the mTORC1-autophagy pathway in the liver and muscle. *J Biol Chem*. 2013;288:21074–21081.
13. **Sinha RA, You SH, Zhou J, et al.** Thyroid hormone stimulates hepatic lipid catabolism via activation of autophagy. *J Clin Invest*. 2012;122:2428–2438.
14. **Sinha RA, Singh BK, Zhou J, et al.** Thyroid hormone induction of mitochondrial activity is coupled to mitophagy via ROS-AMPK-ULK1 signaling. *Autophagy*. 2015;11:1341–1357.
15. **Marsili A, Tang D, Harney JW, et al.** Type II iodothyronine deiodinase provides intracellular 3,5,3′-triiodothyronine to normal and regenerating mouse skeletal muscle. *Am J Physiol Endocrinol Metab*. 2011;301:E818–E824.
16. **Visser WE, Heemstra KA, Swagemakers SM, et al.** Physiological thyroid hormone levels regulate numerous skeletal muscle transcripts. *J Clin Endocrinol Metab*. 2009;94:3487–3496.
17. **Clément K, Viguerie N, Diehn M, et al.** In vivo regulation of human skeletal muscle gene expression by thyroid hormone. *Genome Res*. 2002;12:281–291.
18. **Weitzel JM, Iwen KA, Seitz HJ.** Regulation of mitochondrial biogenesis by thyroid hormone. *Exp Physiol*. 2003;88:121–128.
19. **Short KR, Nygren J, Nair KS.** Effect of T(3)-induced hyperthyroidism on mitochondrial and cytoplasmic protein synthesis rates in oxidative and glycolytic tissues in rats. *Am J Physiol Endocrinol Metab*. 2007;292:E642–E647.
20. **Harper ME, Seifert EL.** Thyroid hormone effects on mitochondrial energetics. *Thyroid*. 2008;18:145–156.
21. **Mullur R, Liu YY, Brent GA.** Thyroid hormone regulation of metabolism. *Physiol Rev*. 2014;94:355–382.
22. **You SH, Liao X, Weiss RE, Lazar MA.** The interaction between nuclear receptor corepressor and histone deacetylase 3 regulates both positive and negative thyroid hormone action in vivo. *Mol Endocrinol*. 2010;24:1359–1367.
23. **Koenig RJ, Smith RJ.** L6 cells as a tissue culture model for thyroid hormone effects on skeletal muscle metabolism. *J Clin Invest*. 1985;76:878–881.
24. **Mizushima N, Yoshimori T, Levine B.** Methods in mammalian autophagy research. *Cell*. 2010;140:313–326.
25. **Mizushima N, Yoshimori T.** How to interpret LC3 immunoblotting. *Autophagy*. 2007;3:542–545.
26. **Scherz-Shouval R, Elazar Z.** Regulation of autophagy by ROS: physiology and pathology. *Trends Biochem Sci*. 2011;36:30–38.
27. **Kakkar P, Singh BK.** Mitochondria: a hub of redox activities and cellular distress control. *Mol Cell Biochem*. 2007;305:235–253.
28. **Zhao J, Brault JJ, Schild A, et al.** FoxO3 coordinately activates protein degradation by the autophagic/lysosomal and proteasomal pathways in atrophying muscle cells. *Cell Metab*. 2007;6:472–483.
29. **Zhang J, Ng S, Wang J, et al.** Histone deacetylase inhibitors induce autophagy through FOXO1-dependent pathways. *Autophagy*. 2015;11:629–642.
30. **Fernandez-Marcos PJ, Auwerx J.** Regulation of PGC-1α, a nodal regulator of mitochondrial biogenesis. *Am J Clin Nutr* 2011;93:884S–890S.
31. **Zhu J, Wang KZ, Chu CT.** After the banquet: mitochondrial biogenesis, mitophagy, and cell survival. *Autophagy*. 2013;9:1663–1676.
32. **Simonides WS, van Hardeveld C.** Thyroid hormone as a determinant of metabolic and contractile phenotype of skeletal muscle. *Thyroid*. 2008;18:205–216.
33. **Jurkuvenaite A, Benavides GA, Komarova S, et al.** Upregulation of autophagy decreases chlorine-induced mitochondrial injury and lung inflammation. *Free Radic Biol Med*. 2015;85:83–94.
34. **Sanchez AM, Bernardi H, Py G, Candau RB.** Autophagy is essential to support skeletal muscle plasticity in response to endurance exercise. *Am J Physiol Regul Integr Comp Physiol*. 2014;307:R956–R969.
35. **Ferraro E, Giammarioli AM, Chiandotto S, Spoletini I, Rosano G.**

Exercise-induced skeletal muscle remodeling and metabolic adaptation: redox signaling and role of autophagy. *Antioxid Redox Signal*. 2014;21:154–176.
36. **Milan G, Romanello V, Pescatore F, et al.** Regulation of autophagy and the ubiquitin-proteasome system by the FoxO transcriptional network during muscle atrophy. *Nat Commun*. 2015;6:6670.
37. **Zhao J, Brault JJ, Schild A, Goldberg AL.** Coordinate activation of autophagy and the proteasome pathway by FoxO transcription factor. *Autophagy*. 2008;4:378–380.
38. **Lo Verso F, Carnio S, Vainshtein A, Sandri M.** Autophagy is not required to sustain exercise and PRKAA1/AMPK activity but is important to prevent mitochondrial damage during physical activity. *Autophagy*. 2014;10:1883–1894.
39. **Bahi L, Garnier A, Fortin D, et al.** Differential effects of thyroid hormones on energy metabolism of rat slow- and fast-twitch muscles. *J Cell Physiol*. 2005;203:589–598.
40. **Qiao S, Dennis M, Song X, et al.** A REDD1/TXNIP pro-oxidant complex regulates ATG4B activity to control stress-induced autophagy and sustain exercise capacity. *Nat Commun*. 2015;6:7014.
41. **Mungai PT, Waypa GB, Jairaman A, et al.** Hypoxia triggers AMPK activation through reactive oxygen species-mediated activation of calcium release-activated calcium channels. *Mol Cell Biol*. 2011;31:3531–3545.
42. **Rahman M, Mofarrahi M, Kristof AS, Nkengfac B, Harel S, Hussain SN.** Reactive oxygen species regulation of autophagy in skeletal muscles. *Antioxid Redox Signal*. 2014;20:443–459.
43. **Schwalm C, Jamart C, Benoit N, et al.** Activation of autophagy in human skeletal muscle is dependent on exercise intensity and AMPK activation. *FASEB J*. 2015;29:3515–3526.
44. **Alers S, Löffler AS, Wesselborg S, Stork B.** Role of AMPK-mTOR-Ulk1/2 in the regulation of autophagy: cross talk, shortcuts, and feedbacks. *Mol Cell Biol*. 2012;32:2–11.
45. **Kim J, Kundu M, Viollet B, Guan KL.** AMPK and mTOR regulate autophagy through direct phosphorylation of Ulk1. *Nat Cell Biol*. 2011;13:132–141.
46. **Peachey LD, Greif RL.** Alterations of mitochondrial structure induced by thyroid hormones in vivo and in vitro. *Endocrinology*. 1965;77:61–77.
47. **Walrand S, Short KR, Heemstra LA, et al.** Altered regulation of energy homeostasis in older rats in response to thyroid hormone administration. *FASEB J*. 2014;28:1499–1510.
48. **Gustafson TA, Markham BE, Morkin E.** Effects of thyroid hormone on α-actin and myosin heavy chain gene expression in cardiac and skeletal muscles of the rat: measurement of mRNA content using synthetic oligonucleotide probes. *Circ Res*. 1986;59:194–201.
49. **Salvatore D, Simonides WS, Dentice M, Zavacki AM, Larsen PR.** Thyroid hormones and skeletal muscle–new insights and potential implications. *Nat Rev Endocrinol*. 2014;10:206–214.
50. **Takikita S, Schreiner C, Baum R, et al.** Fiber type conversion by PGC-1α activates lysosomal and autophagosomal biogenesis in both unaffected and Pompe skeletal muscle. *PloS One*. 2010;5:e15239.
51. **Dentice M, Marsili A, Ambrosio R, et al.** The FoxO3/type 2 deiodinase pathway is required for normal mouse myogenesis and muscle regeneration. *J Clin Invest*. 2010;120:4021–4030.
52. **Branvold DJ, Allred DR, Beckstead DJ, et al.** Thyroid hormone effects on LKB1, MO25, phospho-AMPK, phospho-CREB, and PGC-1α in rat muscle. *J Appl Physiol (1985)*. 2008;105:1218–1227.
53. **Wulf A, Harneit A, Kröger M, Kebenko M, Wetzel MG, Weitzel JM.** T3-mediated expression of PGC-1α via a far upstream located thyroid hormone response element. *Mol Cell Endocrinol*. 2008;287:90–95.
54. **Palikaras K, Lionaki E, Tavernarakis N.** Coupling mitogenesis and mitophagy for longevity. *Autophagy*. 2015;11:1428–1430.
55. **De Palma C, Perrotta C, Pellegrino P, Clementi E, Cervia D.** Skeletal muscle homeostasis in duchenne muscular dystrophy: modulating autophagy as a promising therapeutic strategy. *Front Aging Neurosci*. 2014;6:188.
56. **Wenz T, Rossi SG, Rotundo RL, Spiegelman BM, Moraes CT.** Increased muscle PGC-1α expression protects from sarcopenia and metabolic disease during aging. *Proc Natl Acad Sci USA*. 2009;106:20405–20410.